Journal of Nuclear Materials 382 (2008) 229–241

Contents lists available at ScienceDirect

Journal of Nuclear Materials

journal homepage: www.elsevier.com/locate/jnucmat

Weldable ductile molybdenum alloy development

B.V. Cockeram [a,*], E.K. Ohriner [b], T.S. Byun [b], M.K. Miller [b], L.L. Snead [b]

[a] Bechtel-Bettis Atomic Power Laboratory, P.O. Box 79, West Mifflin, PA 15122-0079, United States
[b] Oak Ridge National Laboratory, Oak Ridge, TN, United States

A B S T R A C T

Molybdenum and its alloys are attractive structural materials for high-temperature applications. However, various practical issues have limited its use. One concern relates to the loss of ductility occurring in the heat-affected weld zone caused by segregation of oxygen to grain boundaries. In this study, a series of arc melted molybdenum alloys have been produced containing controlled additions of B, C, Zr, and Al. These alloys were characterized with respect to their tensile properties, smooth bend properties, and impact energy for both the base metal and welds. These alloys were compared with a very high purity low carbon arc cast molybdenum reference. For discussion purposes the alloys produced are separated into two categories: Mo–Al–B alloys, and Mo–Zr–B alloys. The properties of Mo–Zr–B alloy welds containing higher carbon levels exhibited slight improvement over unalloyed molybdenum, though the base-metal properties for all Mo–Zr–B alloys were somewhat inconsistent with properties better, or worse, than unalloyed molybdenum. A Mo–Al–B alloy exhibited the best DBTT values for welds, and the base metal properties were comparable to or slightly better than unalloyed molybdenum. The Mo–Al–B alloy contained a low volume fraction of second-phase particles, with segregation of boron and carbon to grain boundaries believed to displace oxygen resulting in improved weld properties. The volume fractions of second-phase particles are higher for the Mo–Zr–B alloys, and these alloys were prone to brittle fracture. It is also noted that these Mo–Zr–B alloys exhibited segregation of zirconium, boron and carbon to the grain boundaries.

1. Introduction

Molybdenum and its alloys possess many properties that are of interest for applications at high-temperature. These include high-temperature strength, creep resistance, and relatively low coefficient of thermal expansion [1–2]. One deficiency for most applications is the decreased ductility and increased ductile to brittle transition temperature (DBTT) in the heat-affected zone (HAZ) of welded joints [1–11]. Molybdenum is susceptible to embrittlement when low amounts of oxygen segregates to grain boundaries during recrystallization and grain growth in the HAZ of welds. Alloying molybdenum with small amounts of boron and zirconium has been shown to prevent this grain boundary embrittlement and resulted in improved amounts of ductility in the HAZ of welded TZM [3]. The segregation of zirconium, boron, and carbon to grain boundaries for these Mo–Zr–B alloys resulted in suppressed oxygen concentration at grain boundaries preventing embrittlement in the HAZ of these welds [4,5]. Motivation for that earlier work with Mo–Zr–B alloys was based on earlier efforts by several Russian investigators on similar boron-containing alloys TsM-6 (Mo–Zr–B) and TsM-10 (Mo–Al–B) where improved weld properties were observed [12–14]. The zirconium and/or aluminum may also act as a gettering agent for oxygen.

The objectives of this study are to determine the role of boron and carbon content on the microstructure and mechanical properties of Mo–O.15Zr-B and Mo–Al–B alloys by performing tensile, bend and Charpy impact testing on stress-relieved, recrystallized, and welded specimens. The compositions of the alloys were selected to bound previous work on Mo–Zr–B alloys of 1500 ppm Zr and 6 ppm B and Mo–Al–B alloys of 30 ppm Al and 10 ppm B [3–5,12–14]. Microstructure examinations are performed using metallography, fractography, and atom probe tomography. These results are used to identify the important factors required for improved weldability in this material system.

2. Experimental procedures

2.1. Materials and specimen preparation

The alloys were prepared by vacuum arc remelting (VAR) at ORNL using starting materials of low carbon arc cast (LCAC) molybdenum from H.C. Starck, Cleveland, OH as 6.35 mm thick wrought plate or 38 mm diameter rod [15,16]. Boron powder (<149 μm) of 99.52% ^{11}B (99.9% pure) was obtained from Eagle Picher Technologies LLC. Zirconium wire (99.2% pure) and aluminum wire

* Corresponding author.
E-mail address: cockeram@bettis.gov (B.V. Cockeram).

0022-3115/$ - see front matter © 2008 Elsevier B.V. All rights reserved.
doi:10.1016/j.jnucmat.2008.08.021

(99.999% pure) were procured from Alfa Aesar. Electrodes approximately 1.1 m in length were produced by uniformly distributing these elements along the length of the electrode to produce the alloys summarized in Table 1. Alloy #5 was produced by button melting, crushing the button into coarse powder (repeating this twice), electron-beam melting the powder with LCAC Mo plate to produce rod, and using the 38 mm LCAC Mo rod and Zr wire. A Mo–B–Zr masteralloy for Alloys 1 through 4 was prepared by blending Mo (MMP6 grade from H.C. Starck) and boron powder and placing the mixture into a LCAC Mo tube (3.2 mm OD and 2.2 mm ID) and using 38 mm LCAC Mo rod and Zr wire to melt, extrude and roll into sheet that contained nominally 600 ppm boron.

Table 1
Aim and measured nominal compositions for Mo–Zr–B and Mo–Al–B alloys

Alloy	Position	Composition, ppm				
		B	C	Zr	Al	O
1	Aim	3–9	6–18	750–2250		<10
	Extr @ 20.3 cm	10	7	1400	<1	18
	Extr @ 40.6 cm	17	8	1100	<1	23
	Nominal	14	8	1250	<1	21
2	Aim	3–9	25–75	750–2250	N/A	<10
	Extr @ 20.3 cm	8	26	1900	N/A	20
	Extr @ 40.6 cm	7	23	1500	N/A	13
	Nominal	8	25	1700	N/A	17
3	Aim	12–37	6–18	750–2250		<10
	Extr @ 20.3 cm	14	20	1600	4	14
	Extr @ 40.6 cm	18	24	1700	4	8
	Nominal	16	22	1650	4	11
4	Aim	12–37	25–75	750–2250	N/A	<10
	Extr @ 20.3 cm	54	33	1500	<1	12
	Extr @ 40.6 cm	67	35	1700	<1	7
	Nominal	61	34	1600	<1	10
5	Aim	100–200	25–75	750–2250		<10
	Ingot Top	150	80	1700	<1	11
	Extr @ 20.3 cm	160	62	1700	1	8
	Extr @ 40.6 cm	170	101	1700	<1	9
	Nominal	160	81	1700	<1	9
6	Aim	3–9	25–75		15–45	<10
	Ingot Top	18	55		5	9
	Extr @ 20.3 cm	17	87	28	6	18
	Extr @ 40.6 cm	18	78	34	8	15
	Nominal	18	73	31	6	14
7	Aim	3–9	25–75		100–300	<10
	Extr @ 20.3 cm	1	42	23	47	10
	Extr @ 40.6 cm	1	43	28	55	5
	Nominal	1	43	26	51	8

Alloy	Position	N	Fe	Ni	Si	Cu	Nb	Hf	W	Re	Ta	Ir
	Aim	<10	<50	<20	<50	<10						
1	Nose						2	11	70			
	Tail		10	2	2		2	10	68			1
	Nominal		10	2	2		2	11	69			1
2	Nose		4		1		17	13	13			1
	Tail		3		1		2	14	14	1		1
	Nominal		4		1		10	14	14	1		1
3	Nose		6	1	1	<1	1	12	66	1		
	Tail		6	1	1	<1	1	12	57	<1		
	Nominal		6	1	1	<1	1	12	62	<1		
4	Nose		5		2		2	15	22	2		1
	Tail		5		2		1	16	23	2		1
	Nominal		5		2		2	16	23	2		1
5	Ingot Top	<1	2	<1	2	<1	6	18	33	2		5
	Nose		4	<1	10	<1	5	<1	29	2	<1	4
	Tail		4	<1	5	<1	7	19	34	2	<1	4
	Nominal	<1	3	<1	6	<1	6	13	32	2	<1	4
6	Ingot Top	<1	2	<1	2	<1	4	<1	20	2	<1	3
	Nose		3	<1	2	<1	3	<1	22	2	<1	2
	Tail		4	<1	2	<1	4	<1	22	2	<1	2
	Nominal	<1	3	<1	2	<1	4	<1	21	2	<1	2
7	Nose		3	1	1	<1	1	<1	12	1	<1	3
	Tail		3	1	1	<1	1	<1	10	1	<1	2
	Nominal		3	1	1	<1	1	<1	11	1	<1	3

Measured compositions were determined using combustion analysis at ORNL and GDMS at Shiva.

The electrodes for Alloys 2 and 4 were prepared using the masteralloy sheet with the 38 mm LCAC Mo rod and Zr wire. Alloys 1 and 3 were produced from combining LCAC Mo plate, decarburized by heat treatment in hydrogen at 1600 °C for 72 h, with masteralloy sheet, and Zr wire. Electrodes for Alloys 6 and 7 were prepared by blending Mo and boron powder and placing the mixture in an LCAC Mo tube with Al wire, and using 38mm LCAC Mo rod. The electrodes were VAR melted into a water-cooled copper mold with an initial vacuum of 2×10^{-5} Torr in a Consarc furnace with an average current of 4450–4780 Amps and average voltage of 36.8–38.7 V to produce 88 mm diameter ingots of nominally 15 cm in height. The ingots were extruded at ORNL through a zirconia-coated die using a glass frit lubricant into 51 mm wide × 10–25 mm thick sheet bar at a load of 380–950 tons at a ram rate of 2.5 cm/s after pre-heating to 1350–1400 °C for 1.5 h. The extruded bars were slow cooled in vermiculite.

Portions of the extruded bars were rolled into 1–1.3 mm thick sheet or 4 mm thick plate in air with Mo cover-plates in increments of 10% reduction per pass after pre-heating to temperatures between 800 °C and 1300 °C with final rolling at 600 °C to 400 °C. All materials were machined in the as-worked condition or acid cleaned and stress relieved at 1100 °C prior to machining of test specimens except for Alloy 7, which was stress relieved at 1000 °C. Flat SS-1 dog-bone type tensile specimens (nominally 4.4 cm × 0.5 cm × 0.06 cm) [17] were machined in the longitudinal (L) and transverse (T) orientation. Bend specimens (2.54 cm × 1.27 cm × 0.1 cm) [18], and material for welding were cut from the rolled sheet. Charpy V-notch specimens (25.4 mm × 3.3 mm × 3.3 mm) were machined from the rolled plate in the L-T orientation [19]. The machined specimens were pickled in a solution of 10 parts by volume acetic acid, 4 parts nitric acid, and 1 part HF acid for 5–15 s. to remove 25–51 μm of material [20–22]. Samples were then either tested in the as-worked condition or given a stress relief heat treatment in vacuum (2×10^{-5} Torr at 1100 °C/1 h,) except Alloy 7 (1000 °C/1 h,) or given a recrystallization heat treatment in vacuum for 1 h at 1400 °C for Alloys 1 through 5 and 1300 °C for Alloys 6 and 7. Prior to heat treatment the tensile specimens were electropolished at room temperature in a solution of four parts concentrated sulfuric acid and one part distilled deionized water using a Type 304 stainless steel cathode and a dc voltage of 6–7 V to remove 51–76 μm of material [17]. Commercially produced LCAC sheet material (heat 25732 Ingot 50940, 0.76mm sheet, H.C. Starck) was tested in the stress relieved (850 °C/1 h) or recrystallized (1200 °C/1 h) condition as a control material for tensile testing, bend testing, and welds. The 6.35 mm LCAC plate was used for Charpy testing as a control material.

Chemical analysis of the alloys was performed on sections from the extrusion and in some cases the cast ingot by combustion analysis for carbon and oxygen and Glow Discharge Mass Spectrography (GDMS) for alloying and impurity elements (see Table 1). A consistent loss of aluminum was observed during melting, while little loss of Zr or B was observed. The oxygen levels were generally higher than 10 wppm. The higher oxygen levels may be attributed to the oxygen present in the zirconium addition. The alloying element levels were generally within 50% of aim compositions.

Autogenous electron beam welds were made on sheet coupons that were pickled, ground to a thickness of 1 mm (tensile specimens) or 0.75 mm (bend specimens), and stress relieved prior to welding. Welds for bend specimens made in the direction of rolling at a beam current of nominally 6.4 mA, voltage of 125 kV, filament current of 5 A, chamber pressure less than 1×10^{-4} Torr, and travel speed of 25.4 cm/min. Bend testing of welds was performed with the weld perpendicular to the punch. The weld materials for tensile testing were made normal to the direction of rolling using the same conditions, though with a beam current of 7.3 mA. All bend

specimens were pickled prior to testing, while the tensile specimens were pickled. Tensile specimens also received a stress-relief heat treatment followed by an electropolished prior to testing.

2.2. Testing procedures

Tensile testing was performed at ORNL and Pittsburgh Materials Technology Inc (PMTI), Large, PA at −150 °C to 1000 °C in the longitudinal and transverse orientations for as-worked, stress-relieved, and recrystallized materials in accordance with ASTM E8 methods [23,24]. Tensile testing was performed at a crosshead speed of 0.017 mm/s, corresponding to a nominal strain rate of $\sim$0.0008 s^{-1}. Tensile testing at 200–1000 °C was performed in a vacuum ($<2 \times 10^{-5}$ Torr) furnace equipped with refractory metal grips, heat shields, and heating elements. Testing at subambient temperatures was performed in a chamber that was cooled by liquid nitrogen injection. Heating/cooling times of 30–60 min were typical, and all specimens were soaked at temperature for at least 15 min prior to testing.

Bend testing of smooth specimens was performed at PMTI in 3-point loading using standard procedures [18] with a span of 15t (t is thickness) and a punch radius of 4t. Heating was performed in air and subambient tests were performed using the same methods used for tensile testing. Once the desired temperature was achieved, the punch was placed in contact with the specimen and loaded until the specimen either bent to form an angle of 90° or greater, or fractured at an angle less than 90°. The lowest temperature at which a bend ($\geqslant$90°) was observed was defined as the bend DBTT.

Charpy V-notch impact tests were conducted at ORNL in accordance with the ASTM E23 methods using a Tinius-Olsen 407 J Charpy testing machine [25,26]. An electric heat gun was used for heating to an elevated temperature up to 340 °C in air. The conventional method to analyze the ductile-to-brittle transition using a hyperbolic tangent function could not be applied consistently to all test materials because the transition was too steep for most of the test materials. Therefore, the impact parameters, the DBTT and Upper Shelf Energy (USE), were determined by drawing straight lines in the three temperature ranges: lower shelf, transition, and upper shelf.

Fractographic examinations were performed on some of the tensile specimens using Scanning Electron Microscopy (SEM). Metallographic examinations of microstructure were performed using a Murakami's etch (10 g Potassium Ferri-cyanide + 10 g Potassium Hydroxide + 100 ml water) to reveal the grain structure. Specimens from Alloys #2, #5, and #6 were characterized by atom probe tomography (APT) using the same methods used for earlier work on Mo–Zr–B alloys [4,5,27].

3. Mechanical testing results and discussion

3.1. Tensile testing results

The yield strength and total elongation values determined from tensile testing for LCAC and the Alloys in the Longitudinal As-Worked (LAW), Longitudinal Stress-Relieved (LSR), Longitudinal Recrystallized (LR), and welds are shown in Figs. 1 and 2, respectively. Tensile DBTT values were determined based on the criteria of total elongation of nominally 0.5% or greater, reduction in area greater than 2%, plasticity observed in the load-displacement curves, and ductile features observed at the fracture surface, see Table 2 for a summary of values.

Considering the four metallurgical conditions, the highest yield strength values were observed for the LAW condition with slightly lower yield strength values observed for the LSR condition, and the lowest yield strength values were observed for the LR and weld condition. The high dislocation density for as-worked material likely produces the slightly higher yield strength values. The exception is LCAC plate rolled to sheet at PMTI having slightly lower yield strength values and larger nominal grain thickness (9 μm) than commercially produced LCAC sheet, which can be attributed to the finer grain size of the LCAC sheet (3.9–5.0 μm). The total elongation values for the LAW condition of the respective alloys tended to be the lowest, but a tendency for higher ductility at lower temperatures and lower DBTT values was observed for the LAW condition.

Molybdenum, with its bcc crystal structure and relatively small dislocation core and high Peierls stress barrier for dislocation motion, has a resulting high stress to activate the dislocation sources needed for plastic deformation [31–38]. For this reason molybdenum DBTT is strongly dependent on dislocation density [31–38]. The increased mobile dislocation density for the LAW condition likely lowers the stresses needed to initiate plastic deformation at lower temperatures so that plastic deformation occurs instead of brittle fracture, and a lower DBTT is observed in some cases.

Two different rolling schedules were used to produce the LSR materials with material produced at PMTI at lower rolling temperatures having a slightly higher yield strength, lower total elongation and slightly lower DBTT values in some cases than for LSR material rolled at ORNL. These slight differences in tensile properties likely resulted from the finer grain size and finer particle distributions of the materials rolled at PMTI. However, the slight differences in yield strength and total elongation for the LSR Alloys rolled at PMTI and ORNL suggests that the tensile properties for these alloys are not highly sensitive to subtle changes in microstructure. Recrystallization produces an increase in grain size that results in significantly lower yield strength values compared to the LSR conditions [1–2,6–10,38–41]. Tensile elongation values for LSR were higher than respective values for LAW, while the highest total elongation values were observed for LR. The DBTT values for LSR tended to be slightly higher than observed for LAW with higher values observed for LR that can be attributed to the larger grain size. This relationship between DBTT and grain size is consistent with literature data for wrought molybdenum alloys, where a lower DBTT is observed for alloys with a finer grain size [6–11,20–22,28–38].

Yield strength values for the weld specimens were generally comparable to the values for the recrystallized materials. Since the weld specimens were of uniform cross-section consisting of the weld, HAZ, and base metal, the tensile test of the weld specimen is a measure of the region with the lowest strength. Nearly all failures of the welds occurred in the HAZ. As recrystallization of the base-metal likely occurs in the HAZ, this would explain why the weld strengths are similar to that observed for recrystallized base metal. All weld specimens had DBTT defined as $\sim$200 °C, with the exception of Alloy #6, which was room-temperature (23 °C). Tensile elongation values for the welds at temperatures greater than the DBTT were generally higher than or comparable to LSR values but lower than values for recrystallized material Constraint of plasticity in the HAZ of the weld specimens, which are relatively thin, may limit plastic deformation so that values for total elongation are lower than observed for recrystallized materials. Since the plastic deformation was confined in the weld zone ($\approx$1.5 mm in length) and HAZ ($\approx$0.5–1 mm in length) over the total gauge length used to determine elongation (20.3 mm), the average local strain in the deformed region might be several times higher than the elongation data.

The highest yield strength values were generally observed for the Mo–Zr–B alloys (Alloys #1, #2, #3, #4, and #5), while the yield strength values for the Mo–Al–B alloys (Alloys #6 and #7) tended to be slightly higher than values than LCAC. It is important to note that, for the Mo–Zr–B alloys, a comparatively higher volume

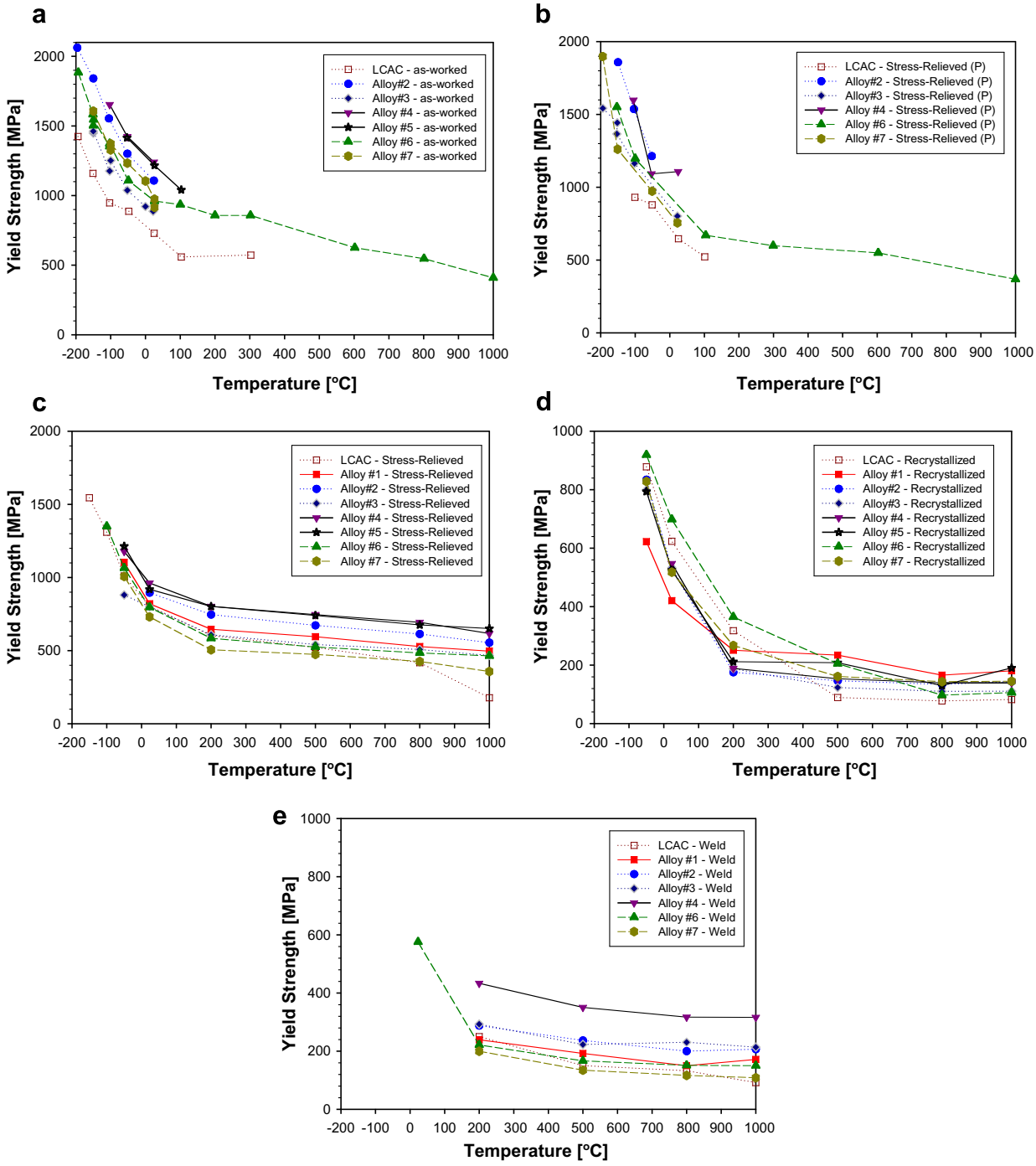

Fig. 1. Comparison of tensile yield strength data determined for LCAC and ORNL Alloys #1, #2, #3, #4, #5, #6, and #7 in the longitudinal orientation for various metallurgical conditions: (a) as-worked, (b) stress-relieved after rolling schedule #2, (c) stress-relieved after primary rolling, (d) recrystallized, and (e) welded. Note the difference in scale for the recrystallized and welded specimens.

fraction of second phase particles was observed. From the literature these second phases are likely borides and carbides. Moreover, one would expect segregation of Zr, boron, and carbon to grain boundaries [3–5]. The higher strength of the Mo–Zr–B alloys is attributed to these microstructural features.

The Mo–Al–B alloys are observed to have a lower volume fraction of second phase particles and boron and carbon are shown by APT to segregate to grain boundaries. These results indicate that the presence of zirconium leads to the formation of a higher volume fraction of second phase particles and additional segregation at grain boundaries resulting in a higher yield strength.

The tensile property trends for the transverse stress-relieved (TSR) orientation was generally similar to that observed for the LSR orientation. Typically, somewhat higher yield strength and lower total elongation values were observed for the TSR orientation compared to the LSR orientation for specific alloys. Similar differences in properties for the TSR and LSR orientation have been observed for wrought unalloyed molybdenum and molybdenum alloys that are attributed to the alignment of grains and second phase particles in the longitudinal orientation with a closer spacing of boundaries in the transverse orientation [1,6–9,20–22,28–30].

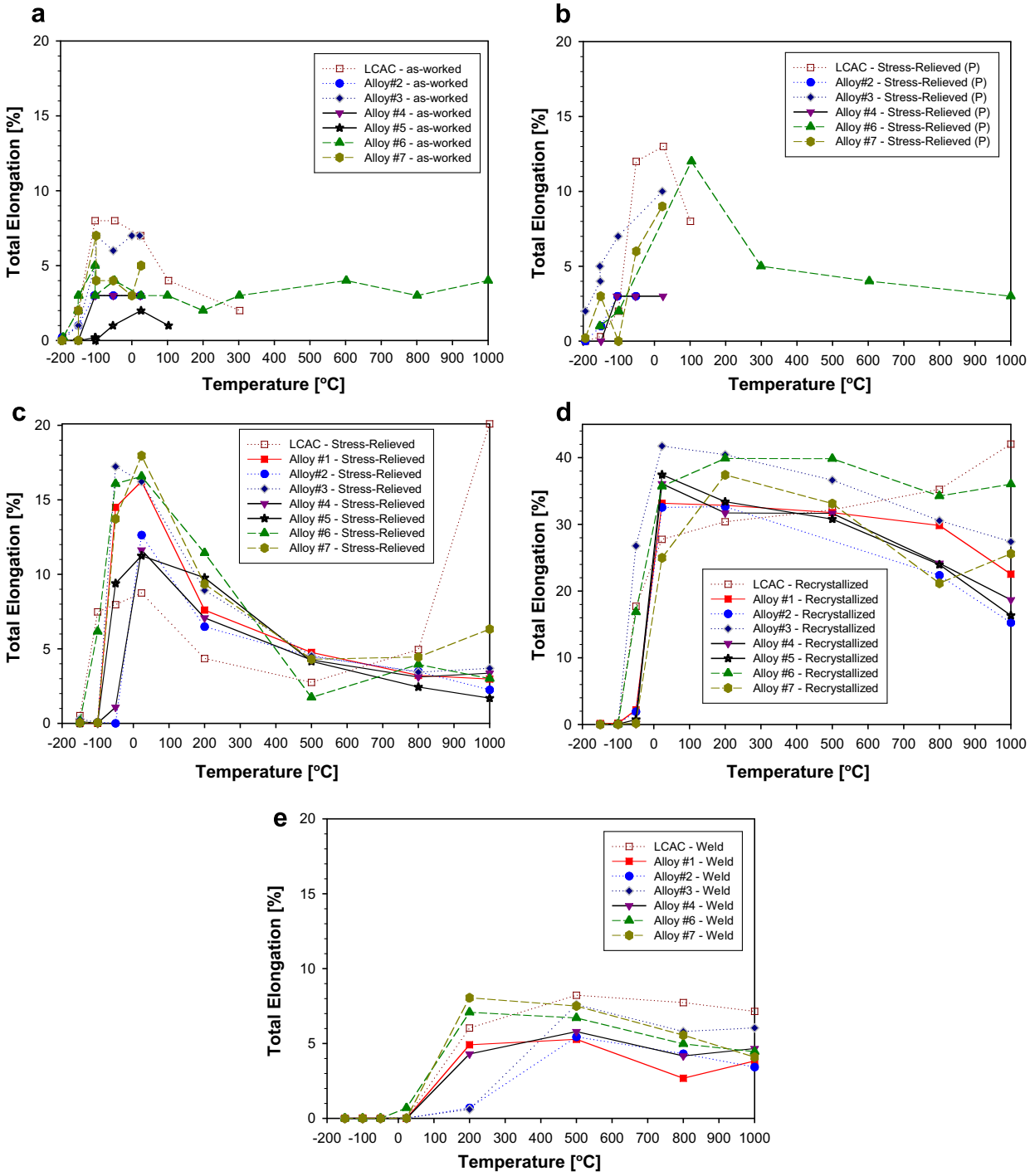

Fig. 2. Comparison of total elongation data determined for LCAC and ORNL Alloys #1, #2, #3, #4, #5, #6, and #7 in the longitudinal orientation for various metallurgical conditions: (a) as-worked, (b) stress-relieved after rolling schedule #2, (c) stress-relieved after primary rolling, (d) recrystallized, and (e) welded. Note the difference in scale for the recrystallized specimens.

SEM fractography provides some insight into the fracture mechanism, and aids in the characterization of the tensile DBTT. Alloy #4 is shown in Fig. 3 to exhibit no ductility and brittle transgranular cleavage features at −150 °C for the as-worked and stress-relieved condition. Testing the same material at −100 °C results in ductile laminate features, plasticity in the load-displacement curves, and measurable ductility. This indicates that the DBTT is between a temperature of −150 °C and −100 °C, but is conservatively defined as −100 °C. As-worked Alloy #5 exhibits low elongation, linear-elastic behavior in the load-displacement curve, and a mixed-mode failure of cleavage and ductile laminate features in Fig. 4 at temperatures as high as −100 °C, while measurable ductility, plasticity in the load-displacement curves, and a fracture surface consisting of more uniform ductile laminate features was observed at −50 °C. This indicates that the tensile DBTT for as-worked Alloy #5 was between −100 °C and −50 °C, but was conservatively defined as −50 °C. As-worked Alloy #6 exhibited low ductility, a linear-elastic load-displacement curve, and brittle-transgranular features in Fig. 5 at −193 °C, while measurable ductility, plasticity in the load–displacement curves and ductile

Table 2
Comparison of DBTT values for LCAC and Alloys #1 through #7 determined from tensile testing for longitudinal as-worked (LAW), longitudinal stress-relieved (LSR) material rolled at PMTI, longitudinal stress-relieved (LSR) material rolled at ORNL, longitudinal recrystallized (LR), longitudinal welded, and transverse stress-relieved (TSR) conditions, smooth bend testing for longitudinal recrystallized and welded materials, and Charpy impact testing for stress-relieved and recrystallized material in the L–T orientation

Material	Tensile DBTT						Bend DBTT		Charpy DBTT (L–T orientation)	
	LAW	LSR-PMTI	LSR	TSR	LR	Weld	LR	Weld	Stress-Relieved	Recryst.
LCAC	−150 °C/ −194 °C	−100 °C/ −150 °C	−100 °C/ −150 °C	–	−50 °C/ −100 °C	200 °C/ 23 °C	−50 °C/ −100 °C	35 °C/ 26 °C	270 °C	247 °C
Alloy #1	–	–	−50 °C/ −100 °C	<−50 °C	−50 °C/ −100 °C	200 °C/ 23 °C	−25 °C/ −49 °C	100 °C/ 75 °C	200 °C	230 °C
Alloy #2	−100 °C/ −150 °C	−100 °C/ −150 °C	23 °C/ −50 °C	23 °C/−50 °C	−50 °C/ −100 °C	200 °C/ 23 °C	−75 °C/ −100 °C	12 °C/ 0 °C	175 °C	255 °C
Alloy #3	−150 °C/ −194 °C	−150 °C/ −194 °C	−50 °C/ −100 °C	<−50 °C	−50 °C/ −100 °C	200 °C/ 23 °C	50 °C/ 23 °C	150 °C/ 100 °C	252 °C	300 °C
Alloy #4	−100 °C/ −150 °C	−100 °C/ −150 °C	−50 °C/ −100 °C	<−50 °C	23 °C/ −50 °C	200 °C/ 23 °C	−75 °C/ −100 °C	23 °C/ 12 °C	260 °C	250 °C
Alloy #5	−50 °C/23 °C	–	−50 °C/ −100 °C	23 °C/−100 °C	23 °C/ −50 °C	–	–	–	300 °C	291 °C
Alloy #6	−150 °C/ −193 °C	−100 °C/ −150 °C	−100 °C/ −150 °C	<−100 °C	−50 °C/ −100 °C	23 °C/ −50 °C	−50 °C/ −75 °C	10 °C/ 0 °C	230 °C	230 °C
Alloy #7	−100 °C/ −150 °C	−50 °C/ −100 °C	−50 °C/ −100 °C	<−50 °C	23 °C/ −50 °C	200 °C/ 23 °C	−50 °C/ −75 °C	100 °C/ 50 °C	235 °C	232 °C

Note: 1. The range of temperatures given for the tensile and bend DBTT values means that ductile behavior was observed at the higher temperature, while brittle behavior was observed at the lower test temperature. The DBTT is between the higher and lower test temperature, but is conservatively define at the higher test temperature. 2. '–' means that results were not obtained for this material/condition.

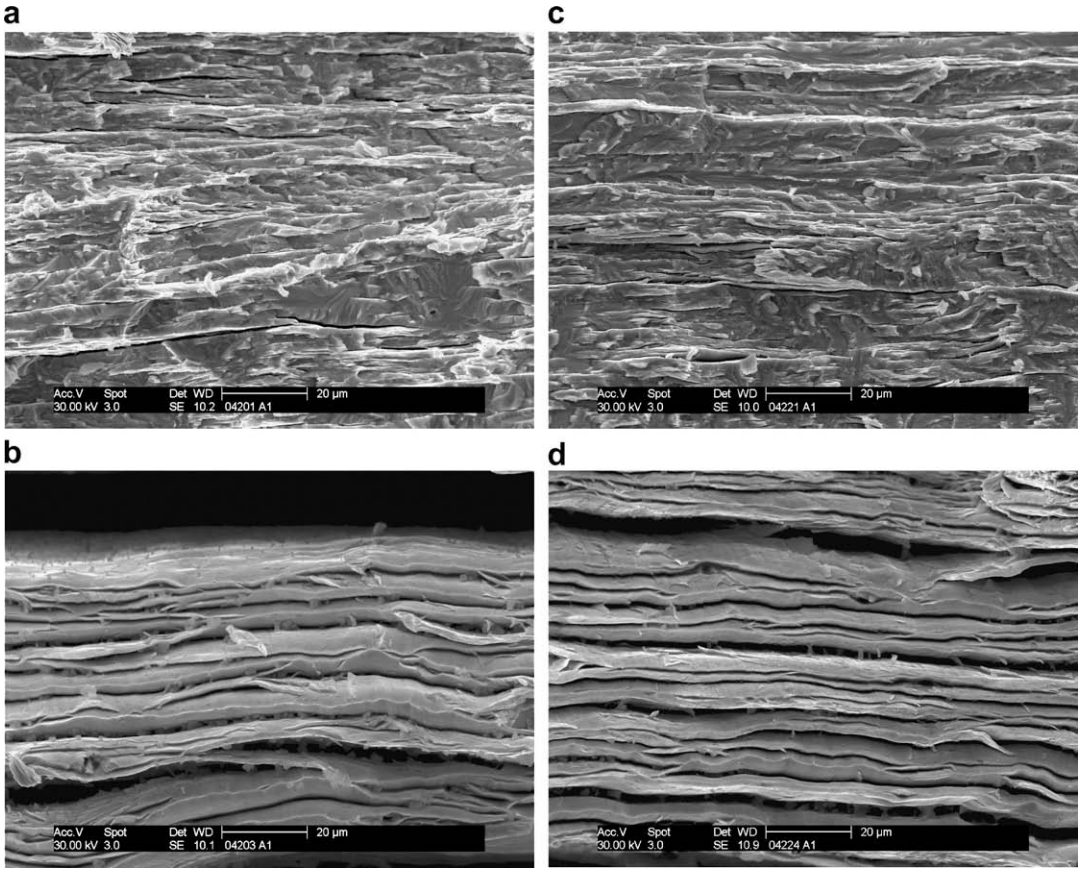

Fig. 3. SEM fractography of Alloy #4 tensile specimens following testing at temperatures close to the DBTT: (a) testing of as-worked material at −150 °C, (b) testing of as-worked at −103 °C, (c) stress-relieved at −150 °C, and (d) stress-relieved at −105 °C.

laminate features were observed at −150 °C. This indicates that tensile DBTT for as-worked Alloy #6 was between −193 °C and −150 °C, but was defined as −150 °C. The ductile-laminate failure mode and microstructure for Alloys #4, #5, and #6 is shown in Fig. 6 to consist of elongated, sheet-like grains similar in shape to those observed for wrought unalloyed molybdenum and other molybdenum alloys [1,2,6–12,20–22]. The ductile laminate failure mode for molybdenum alloys is produced by fracture initiation at grain boundaries that leaves ligaments of sheet-like grains that neck to failure with a high degree of plasticity [20–22]. A low volume fraction of relatively spherical-shaped particles are observed in the microstructure for Alloys #4 and #5 that are presumed to

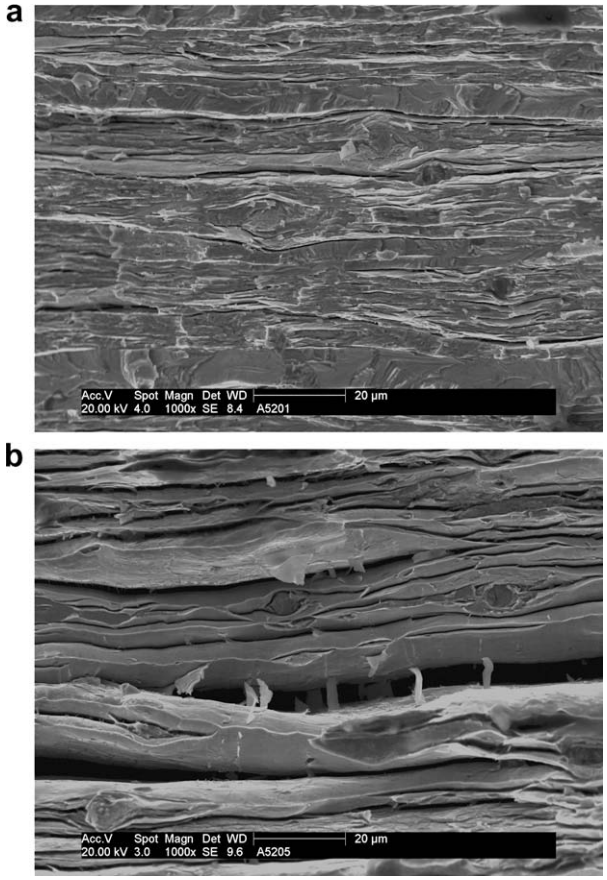

Fig. 4. SEM fractography of as-worked Alloy #5 tensile specimens following testing at temperatures close to the DBTT: (a) testing at −152 °C, and (b) as-worked tested at −53 °C.

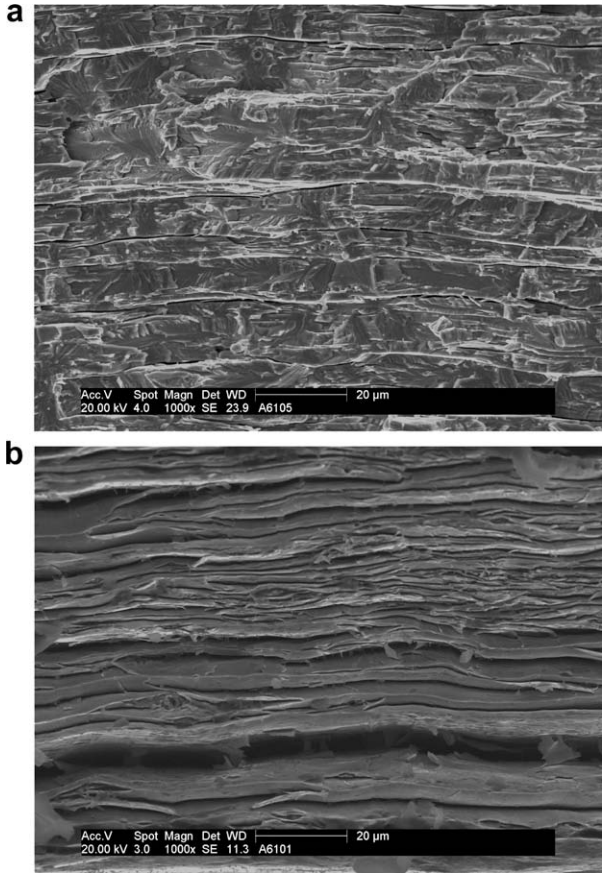

Fig. 5. SEM fractography of as-worked Alloy #6 tensile specimens following testing at temperatures close to the DBTT: (a) testing at −193 °C, and (b) testing of as-worked at −150 °C.

be boride particles, see Fig. 6. Alloy #5 has a higher concentration of boron and a higher fraction of these particles, while Alloy #6 has a lower concentration of boron with no Zr and the lowest fraction of particles. These particles are observed to fracture by a cleavage-type mechanism.

Comparatively higher elongation values and lower DBTT values were observed for LCAC and the Mo–Al–B alloys (Alloy #6 and Alloy #7). A trend toward lower elongation values and higher DBTT values was observed for the Mo–Zr–B alloys (Alloys #1, #2, #3, #4, and #5). The Mo–Zr–B alloys had a higher fraction of particles that were prone to cleavage when the overall fracture mode was either ductile or brittle. The segregation of zirconium, carbon, and boron to grain boundaries expected for the Mo–Zr–B alloys may also limit plastic deformation and explain the higher DBTT values. This suggests that the particles and Zr, B, C segregation present in the Mo–Zr–B alloys are possible fracture initiation sites, and the higher number density of these sites for the Mo–Zr–B alloys likely results in lower elongation and higher DBTT values. The improved ductility and lower DBTT for Alloy #6 compared to the Mo–Zr–B alloys indicate that the additions Al + B do improve the properties of welds, but the concentration of boron and zirconium needs to be low to minimize the volume fraction of particles in the microstructure.

3.2. Smooth bend test results for base metal and welds

The bend DBTT results for the recrystallized base metal are shown in Table 2 to generally be comparable to values determined from tensile tests for LCAC and the Mo–Al–B alloys (Alloys #6 and #7). Bend DBTT results for the Mo–Zr–B alloy base metals (Alloys #1, #2, #3, and #4) were less consistent than the DBTT results obtained from tensile testing. The bend testing method involves the use of a 3-point bend method where the stresses are concentrated at the surface of the specimen opposite the punch, while tensile testing produces uniform stresses along the gage length in the volume of the specimen. Variation in the volume fraction of precipitates in the Mo–Zr–B alloys at the surface of the bend specimen, which act as fracture initiation sites, may lead to more variation in the bend DBTT values. LCAC and the Mo–Al–B alloys have a low volume fraction of second phase precipitates, which lead to more consistent DBTT values determined using the bend and tensile test. The bend DBTT values for the Alloy #2 and #4 base metal were slightly lower than measured for LCAC and Alloy #6. These results indicate that higher amounts of carbon with either lower or a mid-range of boron, possibly with some amount of aluminum, is needed for a recrystallized molybdenum alloy to have DBTT values comparable to LCAC Mo in the case of Alloy #6, or slightly better than LCAC Mo in the case of Alloys #2 and #4.

As seen in Fig. 7, the DBTT values for the welds were consistently higher than the base metals for all alloys. The bend testing DBTT values for the welds were generally consistent with the tensile DBTT values with the DBTT for Alloy #6 below room temperature while the bend DBTT values for LCAC and all other alloys was between room-temperature and 200 °C. The exception is the bend DBTT results for Alloy #2 (12 °C) being below room-temperature. Alloy #6 had the lowest bend DBTT (10 °C) compared to LCAC (35 °C) and all other alloys. These results indicate that low additions of boron and Al produces a low volume fraction of second phase particles and grain boundary segregation of boron perhaps resulting in reduced DBTT for the welds. The higher bend DBTT

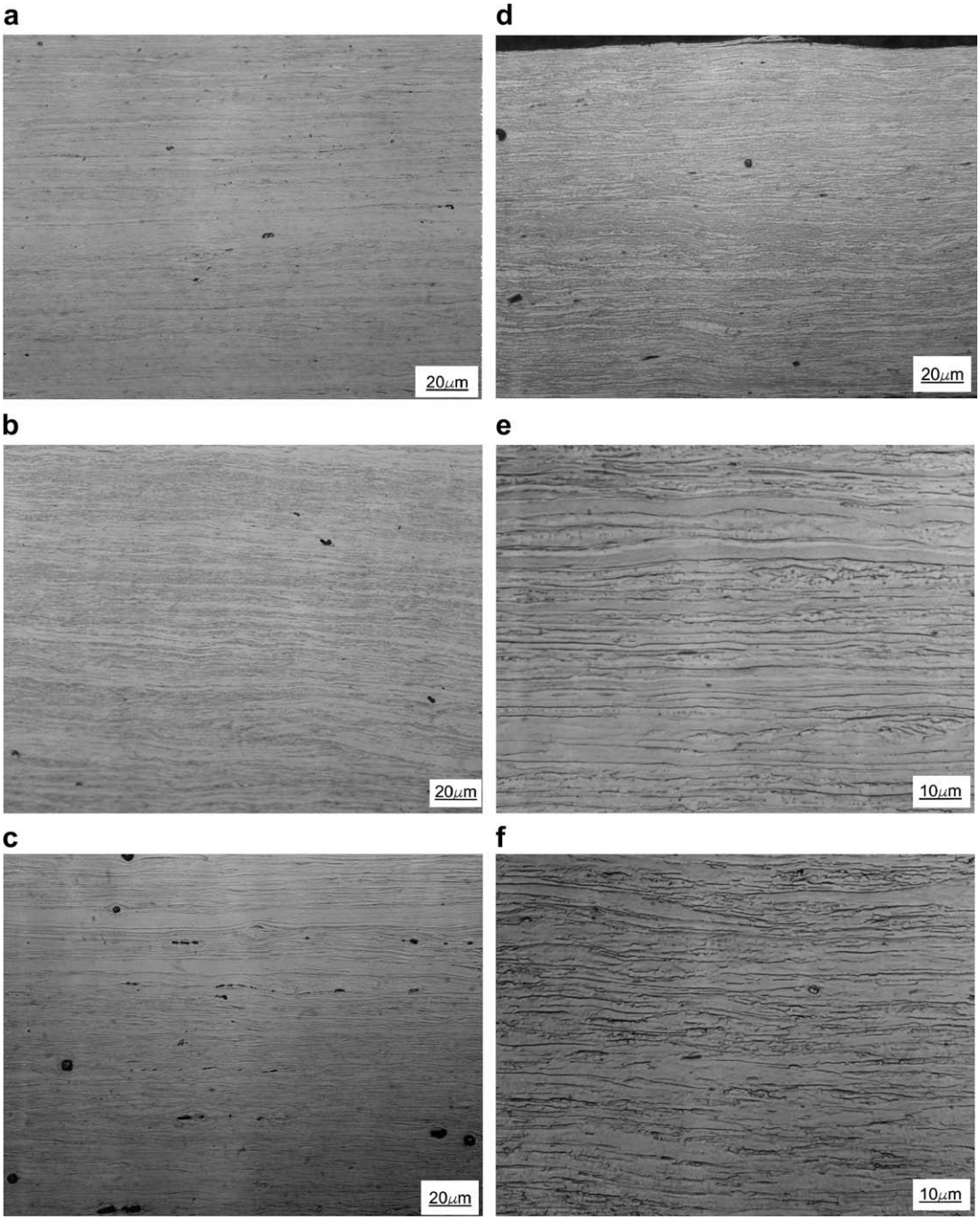

Fig. 6. Optical metallography of the microstructure of Alloy #4, #5, and #6 in the as-worked condition: (a) Alloy #4 in the longitudinal orientation, (b) Alloy #4 in the transverse orientation, (c) Alloy #5 in the longitudinal orientation, (d) Alloy #5 in the transverse orientation, (e) Alloy #6 in the longitudinal orientation at twice the magnification of the images for Alloy #4 and #5, and (f) Alloy #6 in the transverse orientation.

for the Alloy #7 weld in comparison to Alloy #6 may be attributed to the higher Al and lower boron content. The bend DBTT for the Alloy #2 (12 °C) and Alloy #4 (23 °C) welds were also slightly lower than observed for LCAC. This result indicates that the addition of zirconium and boron results in improved damage tolerance for molybdenum welds that is similar to that reported for Mo–Zr–B alloys [3–5] and may be attributed to the segregation of zirconium, boron, and carbon to grain boundaries. Much higher weld DBTT values were observed for the welds from Alloys #1 and #3 that appear to be attributed to the lower carbon content. Carbon was also observed to segregate to grain boundaries with zirconium and boron to provide improved fracture resistance for Mo–Zr–B alloys [3–5]. A low ratio of carbon to oxygen content has been reported in literature to result in a higher tendency for the grain boundary embrittlement in molybdenum [6–8,39–42], and may explain the high DBTT values for Alloys #1 and #3. This suggests that some carbon may be required along with the boron to provide a slight improvement in the fracture resistance of welds.

3.3. Charpy impact testing results for base metal

Plots of Charpy impact energy versus temperature for the stress-relieved and recrystallized condition are seen in Figs. 8 and 9, respectively, with a summary of the DBTT values and Upper Shelf Energy (USE) values provided in Table 3. The DBTT values determined from Charpy testing are shown in Table 2 to be

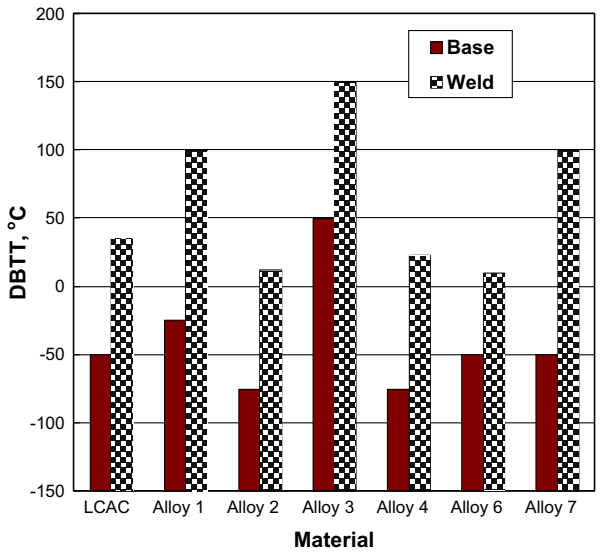

Fig. 7. The DBTT values determined from the smooth bend testing of recrystallized base metals and autogenous electron beam welds. All specimens are in the longitudinal orientation. The weld is along the length of the specimen and perpendicular to the punch.

consistently higher than determined from tensile testing or smooth bend testing due to the constraining effect of a notch. Metals having a bcc crystal structure such as steels and molybdenum are known to have notch sensitivity under a triaxial stress-state leading to a higher DBTT [41–46]. Fracture toughness testing has revealed a similar trend for LCAC Mo where toughness DBTT values of 150–200 °C were determined from fracture toughness testing compared to DBTT values determined from tensile testing that range from room-temperature to −100 °C [20–22]. Moreover, Charpy impact tests are performed at a much higher strain rate compared to fracture toughness tests. The DBTT for metals with a bcc structure are known to be highly sensitive to strain rate, with testing at a higher strain rate producing a higher DBTT [36–45]. However, Charpy test results can be used for comparison to identify the alloys with improved impact resistance.

Considering the stress-relieved condition, only alloys #3, #6, and #7 have USE values (11.9 to 16.6 J) that are higher than measured for LCAC (9.9 J). The Charpy DBTT for stress-relieved Alloys #3, #6, and #7 occurred over a very narrow temperature range and were slightly lower than determined for stress-relieved LCAC. Although the USE values for stress-relieved Alloys #1, #2, and #4 were generally lower (3.1 J and less) and the DBTT values occurred over a larger range of temperature, the Charpy DBTT values were also slightly lower than LCAC. The lowest USE and highest DBTT was observed for Alloy #5, which likely results from the high volume fraction of brittle second phase particles. Alloys #6 and #7 contain low levels of boron and carbon with little zirconium that results in the presence of a much lower volume fraction of brittle second phase particles, though enough boron is present to provide beneficial strengthening of the grain boundaries compared to LCAC. The Mo–Zr–B alloys (Alloys #1, #2, #3, and #4) likely have the benefit of Zr + B + C segregation to grain boundaries that generally improves the cohesion energy of boundaries and results in slightly lower DBTT values compared to LCAC.

For the recrystallized alloys, the USE values for all alloys (10.8–13.8 J) were higher than LCAC (9.2 J), with Alloys #1, #6, and #7 exhibiting slightly lower DBTT as compared to LCAC. Alloys #6 and #7 exhibited a small decreases in USE for the recrystallized condition compared to the stress-relieved condition, but no change in DBTT was observed for Alloys #6 and #7 after recrystallization. The higher USE and lower DBTT for Alloy #6 and #7 in the stress-relieved and recrystallized conditions compared to LCAC shows that small additions of B and Al produce slight improvements in the impact resistance compared to unalloyed molybdenum. The USE for the recrystallized Mo–Zr–B Alloys was generally higher than the respective values for the stress-relieved condition, though the DBTT values for the recrystallized alloys were generally higher than respective values for the stress relieved alloys. An exception was Alloy #3, where the USE for recrystallized material was lower than observed for the stress-relieved condition. The DBTT values for recrystallized Alloy #1 (230 °C) was lower than for recrystallized LCAC (247 °C) while the DBTT values for Alloys #2 and #4 (255 °C and 250 °C) were slightly higher. These results suggest that the addition of boron and zirconium can provide improved impact resistance and fracture resistance relative to unalloyed molybdenum, but the carbon and boron levels need to be kept low so that the formation of particles that exhibit brittle behavior is not observed. These particles are fracture initiation sites and exhibit brittle cleavage. Alloy #1 had the lowest carbon and boron content of all Mo–Zr–B alloys, which may result in the lowest volume fraction of particles and result in DBTT values that are slightly lower than LCAC.

4. Microstructure examinations and role of alloying

Atom probe tomography (APT) was performed on stress-relieved Alloys #2, #5, and #6 to determine if the segregation of zirconium, boron, and carbon to grain boundaries that was previously observed [3–5] was also present in these alloys. Unfortunately it proved difficult to image a grain boundary in atom probe (due to the large grain sizes) for Alloys #2 and #5. However, a grain edge-on view for Alloy 6 is provided in Fig. 10, clearly indicating enrichment of boron and carbon. Moreover, a small amount of randomly distributed aluminum (50 ± 14 ppm) was detected within the grain, consistent with the bulk composition indicating that aluminum had not segregated (Fig. 10.) The level of oxygen detected at the boundary and matrix was at background levels. As mentioned previously, an alloy similar to that of Alloy #6 was studied by atom probe tomography, indicating the segregation of boron at the grain boundaries in the absence of zirconium also prevents the segregation of oxygen to grain boundaries [3–5]. Given the slightly lower Charpy DBTT values than LCAC and a slightly lower weld DBTT such an exclusion of oxygen from the grain boundary due to the presence of boron, zirconium, and carbon is very plausible.

Analysis of the matrix of the grain regions for Alloys #2 and #5 detected mainly zirconium, boron, and carbon at concentrations consistent with the bulk composition. Based on previously reported atom probe tomography for Mo–Zr–B alloys [3–5], the segregation of boron, carbon, and zirconium would be expected to be present. The properties measured in the present work for the Mo–Zr–B base do not show clear trends towards improved performance, with results both superior and inferior to the LCAC standard depending on the alloy variant. As example, slightly lower bend DBTT values were observed for Alloy #2 and Alloy #4 welds compared to LCAC, while the Charpy DBTT values for stress-relieved Alloys #2 and #4 were generally a small improvement over LCAC with the exception of slightly higher Charpy DBTT values observed for Alloys #2 and #4 in the recrystallized condition. The higher DBTT values observed for Alloys #1 and #3 suggest that higher levels of carbon, and possibly boron, need to be present in Mo–Zr–B alloys to enhance alloy or weldment ductility. Alloy #5 possessed the highest boron content and resulted in the highest volume fraction of brittle particles present, resulting in the poorest fracture resistance. The higher levels of zirconium, carbon and boron present for the Mo–Zr–B alloys compared to Alloy #6 results in the formation of a higher number density of brittle particles resulting in a decreased resistance to brittle fracture. Based on these results it is suggested that segregation of

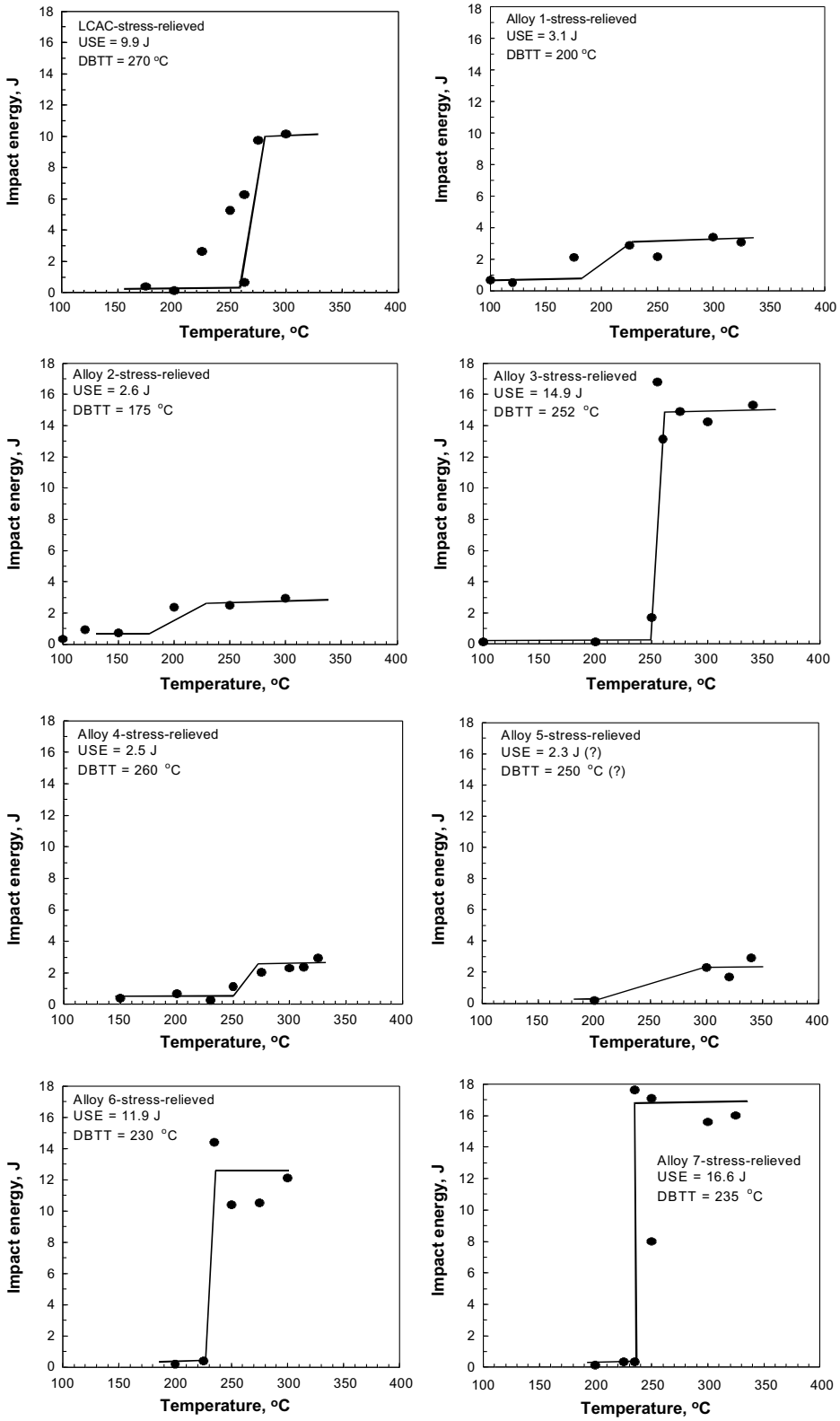

Fig. 8. Plots of Charpy impact energy versus temperature for the stress-relieved Mo-alloys in the L–T orientation with the DBTT and USE values identified.

zirconium to grain boundaries for the Mo–Zr–B alloys produces less fracture resistance. Moreover, improved properties in the HAZ of molybdenum welds can be achieved by the addition of boron and carbon on the level of that present in Alloy #6 (nominally 20 ppm or less boron with 50-100 ppm carbon) and by limiting the zirconium content.

5. Summary and conclusion

Alloys of molybdenum containing controlled additions of Al, Zr, B and C were produced and compared to a high purity LCAC molybdenum. The majority of these alloys exhibited improved strength which is attributed to the presence of second phase particles (likely

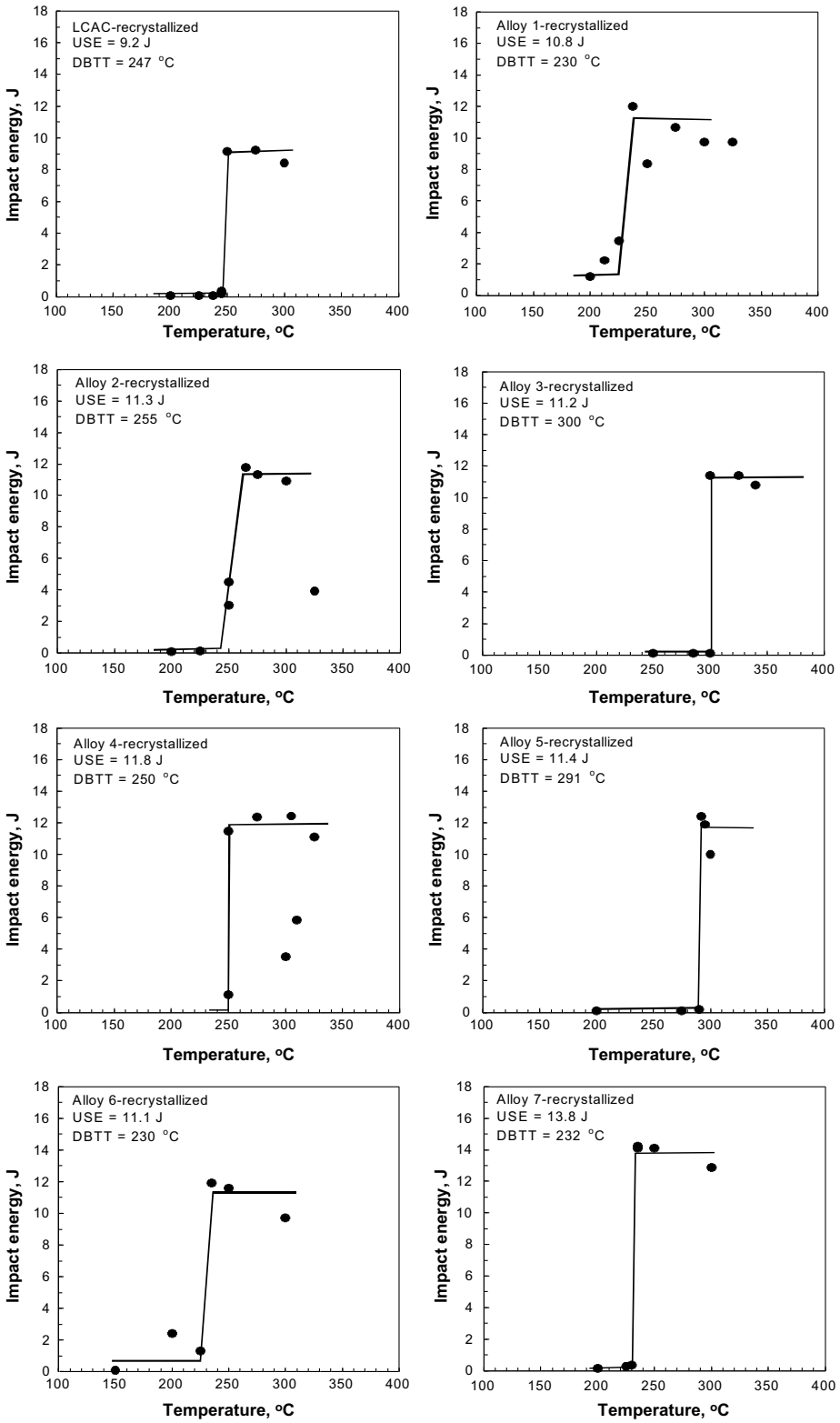

Fig. 9. Plots of Charpy impact energy versus temperature for the recrystallized Mo-alloys in the L–T orientation with the DBTT and USE values identified.

carbides or borides) and the segregation of zirconium, boron, and carbon to grain boundaries. However, further study to make this conclusion is necessary. A low number density of particles was observed for the Mo–Al–B alloys and only boron and carbon was observed to have segregated to grain boundaries which resulted in tensile strength values that were comparable to, or higher than those observed for LCAC. The tensile elongation values for the Mo–Zr–B alloys tended to be lower than LCAC and the Mo–Al–B alloys, and the DBTT values for the Mo–Zr–B alloys were comparable to or higher than LCAC and the Mo–Al–B alloys. The Mo–Zr–B alloys were prone to the formation of brittle particles leading to cleavage and segregation of zirconium, carbon, and boron to grain

Table 3
Summary of Charpy impact testing results for LCAC and Alloys #1 through #7 in the stress-relieved and recrystallized conditions in the L–T orientation

Material	Results for stress-relieved condition		Results for recrystallized condition	
	DBTT (°C)	USE (J)	DBTT (°C)	USE (J)
LCAC	270	9.9	247	9.2
Alloy #1	200	3.1	230	10.8
Alloy #2	175	2.6	255	11.3
Alloy #3	252	14.9	300	11.2
Alloy #4	260	2.5	250	11.8
Alloy #5	300	2.3	291	11.4
Alloy #6	230	11.9	230	11.1
Alloy #7	235	16.6	232	13.8

The plots of impact energy versus test temperature are given in Figs. 8 and 9.

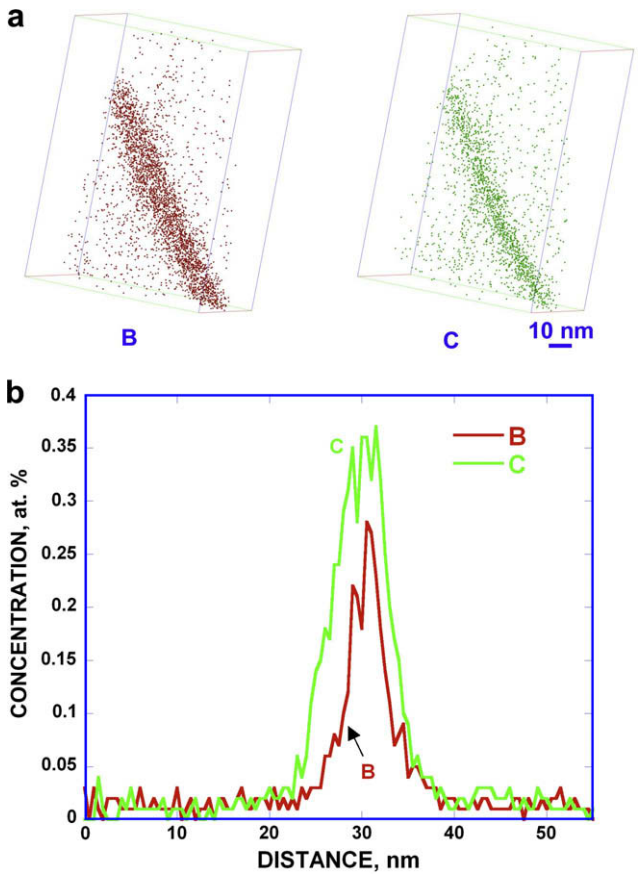

Fig. 10. Atom probe analysis of Alloy #6 in the stress-relieved condition showing the segregation of boron and carbon at a grain boundary: (a) atom maps for boron and carbon at a grain boundary, and (b) concentration profiles for boron and carbon through the matrix and grain boundary showing the segregation of boron and carbon at the grain boundary.

boundaries, also speculated to limit the ductility of these alloys. These factors likely result in the less consistent DBTT values for the Mo–Zr–B alloys compared to LCAC molybdenum where the DBTT values for Mo–Zr–B alloys were in some cases a clear improvement over the LCAC molybdenum standard. The total elongation and DBTT for the Alloy #6 base material were generally comparable to LCAC, or slightly better. The higher DBTT for Alloy #7 indicates that higher aluminum and lower boron contents as compared to Alloy #6 are not desirable. Boron concentrations on the order of 10–20 ppm are likely most beneficial in combination with low amounts of zirconium to minimize the formation of brittle particles and to enhance the segregation of boron and carbon to grain boundaries.

The clearest impact of the alloying addition is on the properties of the weldment. Two of the Mo–Zr–B alloys (Alloys #2 and #4) had slightly lower bend DBTT values (12 °C and 23 °C) as compared to LCAC molybdenum welds (35 °C), though the Charpy impact properties for the Mo–Zr–B alloys did not exhibit consisted improvement. The Mo–Zr–B alloys with a low carbon content (Alloys #1 and #3) exhibited higher weld DBTT values as compared LCAC molybdenum. This suggests higher levels of carbon are needed for improved weld properties. Segregation of boron, carbon, and zirconium to grain boundaries is believed to displace oxygen from grain boundaries [3–5] leading to improved properties for welds. The lowest weld DBTT values were observed for Alloy #6 (a Mo–Al–B alloy) and the Charpy impact properties were consistently better as compared to the LCAC molybdenum standard. This alloy exhibited only boron and carbon segregation to the grain boundaries with a low fraction of embrittling particles.

Segregation of boron and carbon to grain boundaries is speculated to be mechanism responsible for the displacement of oxygen from the grain boundaries. Within the limited set of alloys studied in this work, it is also speculated that elevated levels of zirconium has led to the formation of brittle second phase particles and therefore should be avoided.

Acknowledgements

This work was supported under USDOE Contract No. DE-AC11-98PN38206. Atom probe tomography was carried out at the Oak Ridge National Laboratory SHaRE User Facility, which is sponsored by the Office of Basic Energy Sciences, Division of Scientific User Facilities, US Department of Energy, under Contract DE-AC05-00OR22725 with UT-Battelle, LLC.

References

[1] J.B. Lambert, J.J. Rausch. Non-Ferrous Alloys and Special-Purpose Materials, Materials Handbook, vol. 2, ASM International, Materials Park, OH, 1992, pp. 557–582.
[2] R.E. Gold, D.L. Harrod, J. Nucl. Mater. 85 (1979) 805.
[3] A.J. Bryhan, Welding Research Council Bulletin 312, United Engineering Center, NY, February 1986, ISSN 0043-2326.
[4] M.K. Miller, E.A. Kenik, M.S. Mousa, K.F. Russel, A.J. Bryhan, Scr. Metall. 46 (2002) 299.
[5] M.K. Miller, A.J. Bryhan, Mater. Sci. Eng. A 327 (2002) 80.
[6] J. Wadsworth, T.G. Nieh, J.J. Stephens, Int. Mater. Rev. 33 (3) (1988) 131.
[7] A. Kumar, B.L. Eyre, Proc. Royal Soc. London A370 (1980) 431.
[8] J. Wadsworth, T.G. Nieh, J.J. Stephens, Scr. Metall. 20 (1986) 637.
[9] J.R. Stephens, W.R. Witzke, J. Less Common Met. 29 (1972) 371.
[10] J.B. Brosse, R. Fillit, M. Biscondi, Scr. Metall. 15 (1981) 619.
[11] A. Suzuki, H. Matsui, H. Mimura, Mater. Sci. Eng. A 47 (1981) 209.
[12] N.N. Morgunova, L.N. Demina, N.I. Kazakova, Met. Sci. Heat Treat. (USSR) 28 (11&12) (1986) 895.
[13] V.V. Bukhanovskii, N.G. Kartyshov, E.G. Polishchuk, V.K. Karchenko, M.I. Chikunov, Strength Mater. (USSR) 19 (8) (1987) 1093.
[14] M.M. Nerodenko, E.P. Polishchuk, Y.U.I. Demkin, A.I. Senin, G.V. Fetisov, Automat. Weld. (USSR) 32 (6) (1979) 52.
[15] Standard Specification for Molybdenum and Molybdenum Alloy Plate, Sheet, Strip, and Foil, ASTM B386-91, American Society for Testing and Materials, Philadelphia, PA, 1997.
[16] Standard Specification for Molybdenum and Molybdenum Alloy Bar, Rod, and Wire, ASTM B386-95, American Society for Testing and Materials, Philadelphia, PA, 1995.
[17] B.V. Cockeram, J.L. Hollenbeck, L.L. Snead, J. Nucl. Mater. 324 (2004) 77.
[18] Refractory Metal Sheet Rolling Panel, "Evaluation of Test Methods for Refractory Metal Sheet Material", Materials Advisory Board, National Academy of Sciences – National Research Council, MAB-192-M, April 22, 1963.
[19] Standard Terminology Relating to Fatigue and Fracture Testing, ASTM E1823-96, American Society for Testing and Materials, Philadelphia, PA, 1996.
[20] B.V. Cockeram, Metall. Trans. 33A (2002) 3685.
[21] B.V. Cockeram, Metall. Trans. 36A (2005) 1777.
[22] B.V. Cockeram, Mater. Sci. Eng. A 418 (2006) 120.
[23] Standard Test Methods for Tension Testing of Metallic Materials, ASTM E8-01, American Society for Testing and Materials, Philadelphia, PA, 2001.
[24] Standard Test Methods for Elevated Temperature Tension Tests of Metallic Materials, ASTM E21-98, American Society for Testing and Materials, Philadelphia, PA, 1998.

[25] Standard Test Methods for Notched Bar Impact Testing of Metallic Materials, ASTM E23-98, American Society for Testing and Materials, Philadelphia, PA, 1998.
[26] Alexander, DJ; Nanstad, RK; Corwin, WR; Hutton, JT, in: AA Braun, NE Ashbaugh, FM Smith, (Eds.), Applications of Automation Technology to Fatigue and Fracture Testing, ASTM STP 1092, American Society for Testing and Materials, Philadelphia, 1990, pp. 83–94.
[27] M.K. Miller, Atom Probe Tomography: Analysis at the Atomic Level, Academic/Plenum Press, New York, 200, p. 1.
[28] J. Wadsworth, C.M. Packer, P.M. Chewey, W.C. Coons, Metall. Trans. 15A (1984) 1741.
[29] J.A. Shields, P. Lipetzky, A.J. Mueller, in: G. Kneringer, P. Rodhammer, H. Wildner (Eds.), Proceedings of the 15th International Plansee Seminar, Powder Metallurgical High Performance Materials Proceedings, vol. 4, Plansee Holding AG, Reutte, Austria, 2001, pp. 187–199.
[30] D.L. Chen, B. Weiss, R. Stickler, M. Witwer, G. Leichtfried, H. Hödl, High Temp. Mater. Process. 13 (1994) 75.
[31] ASM Metals Handbook, 9th Ed., vol. 3, American Society for Metal, Metals Park, OH, 1980, p 328.
[32] G.T. Hahn, Acta Metall. 10 (1962) 727.
[33] F.P. Bullen, H.L. Wain, in: Proceedings of the First International Conference on Fracture, Japanese Society for Strength of Materials, Japan, 1966, p. 1933.
[34] M.F. Ashby, J.D. Embury, Scr. Metall. 19 (1985) 557.
[35] A. Seeger, E. Donth, S. Pfaff, Disc. Faraday Soc. 23 (19) (1957).
[36] W.G. Johnston, J.J. Gilman, J. Appl. Phys. 30 (129) (1959).
[37] W.G. Johnston, J. Appl. Phys. 33 (2716) (1962).
[38] F.A. McClintock, A.S. Argon, Mechanical Behavior of Materials, Addison-Wesley, New York, 1965. pp. 152–214.
[39] M. Semchyshen, R.Q. Barr, J. Less Common Met. 11 (1966) 1.
[40] M. Semchyshen, R.Q. Barr, Arc-cast molybdenum-base alloys, Climax Molybdenum Company of Michigan, Contract No. N8onr-78,700, Summary Report, 1955.
[41] J. Wadsworth, J.P. Wittenauer, in: E.N.C. Dalder, T. Grobstein, and C.S. Olsen, Evolution of Refractory Metals and Alloys, TM, Warrendale, PA, 1994, pp. 85–108.
[42] W.D. Klopp, J. Less Common Met. 42 (1975) 261.
[43] R.W. Hertzberg, Deformation and Fracture Mechanics of Engineering Materials, 2nd Ed., John Wiley and Sons, New York, 1983. pp. 269–348.
[44] C. Grandhi, M.F. Ashby, Acta Metall. 27 (1979) 1565.
[45] A. Lawley, J. Van den Sype, R. Maddin, J. Inst. Met., vol. 91, 1962–1963, pp. 23–27.
[46] G.W. Brock, Trans. Met. Soc. AIME 221 (1961) 1055.